Instability of steady states with inhomogeneous field in electron–positron plasma diode

View Online   Export Citation   CrossMark

L. A. Bakaleinikov,[a)] iD V. I. Kuznetsov,[b)] iD E. Yu. Flegontova,[c)] iD D. P. Barsukov,[d)] iD and I. K. Morozov[e)] iD

AFFILIATIONS

Ioffe Institute, St. Petersburg 194021, Russia

[a)]Electronic mail: bakal51@mail.ru
[b)]Author to whom correspondence should be addressed: victor.kuznetsov@mail.ioffe.ru
[c)]Electronic mail: fl.xiees@mail.ioffe.ru
[d)]Electronic mail: bars.astro@mail.ioffe.ru
[e)]Electronic mail: morozov22505@gmail.com

ABSTRACT

Instability features of steady states of the plasma diode with electron and positron counter flows are studied. There are several types of such states for each value of the inter-electrode distance. The case when charged particles moving in the diode plasma are not reflected from potential extrema is considered. We have solved an equation for the amplitude of the electric field perturbation for steady states with an inhomogeneous field distribution. Studying the dispersion equation has shown that all considered solutions are unstable. We have also confirmed this result when simulating small perturbation evolution of a steady-state solution.

Published under an exclusive license by AIP Publishing. https://doi.org/10.1063/5.0168756

I. INTRODUCTION

Plasma consisting of electrons and positrons is found in many high-energy astrophysical objects, such as neutron stars and their environment, black holes and active galactic nuclei, relativistic jets that produce bursts of gamma rays, etc. In an attempt to better understand their properties, a large number of theoretical works and a number of laboratory experiments have been carried out, see, for example, the review of Ref. 1. An example of the most complex astrophysical objects containing electron-positron plasma are pulsars. They were discovered more than 50 years ago, but there is still no clear idea of either the mechanism of their radiation or the reason for the jump between modes; see, for example, Ref. 2. The pulsar radio emission generation is usually assumed to be related to growing instabilities in the electron–positron plasma at some altitude above the pulsar diode, where the longitudinal electric field is completely screened by plasma, see, for example, Refs. 3–5. In recent years, it was supposed that the origin of pulsar radio radiation may be related to collective processes in electron–positron plasma inside the pulsar diode itself, see, for example, Refs. 6 and 7. In particular, the model that pulsar radio radiation is produced directly inside the pulsar diode has been considered in Refs. 8 and 9. In this regard, the study of the operating modes of plasma diodes is of great interest.

The stationary states of a plasma diode with counter flows of electrons and positrons were studied in Ref. 10, and studying features of

their stability was started in Ref. 11. Instability of steady states is characteristic of the diodes with collisionless plasma. The mechanism of instability development is the same as that of the known Pierce instability where a beam of electrons moves in the space of a diode against a background of stationary ions.[12] It should be noted that collective effects in electron–positron plasma, created by a laser beam were considered, for example, in Ref. 13, and instabilities in such a plasma were studied in Refs. 14–16.

The steady states of a vacuum diode with counter flows of electrons and positrons coming from opposite boundaries can be divided into two main types depending on the nature of the motion of charged particles: (1) all particles reach the opposite electrode, and (2) part of the particles is reflected from the potential barrier inside the diode and returns to the electrode they are emitted from.[10] In Ref. 11, an equation for electric field perturbation for stationary solutions of the first type is derived. In addition, in Ref. 11, an analytical solution of this equation is found for a homogeneous field distribution, a dispersion equation is obtained, and dispersion branches are constructed. It is proved that homogeneous solutions are stable for the values of the inter-electrode gap less than $\sqrt{2}\,\pi\,\lambda_D$, where λ_D is the Debye–Hückel length.

In the present paper, the stability features of inhomogeneous stationary solutions of the first kind are studied. The solution of equation for amplitude of electric field perturbation is found by using a semianalytical approach. The dispersion equation is derived, and its solutions

22 January 2024 12:51:34

are studied. It is shown that all considered inhomogeneous stationary states are unstable with respect to small perturbations. In addition to that the evolution of small perturbations of electric field distribution in the initial state is studied numerically using two codes: EK-code and PIC-code. The results of numerical calculations of initial stage of perturbation evolution are compared with analytical ones.

II. STATIONARY SOLUTIONS AND FIELD PERTURBATION EQUATION

Following Ref. 11, we assume that monoenergetic electron beam comes from the left electrode with number density $n_{e,0}$ and nonrelativistic velocity $v_{e,0}$, and monoenergetic positron beam comes from the right electrode with number density $n_{p,0} = n_{e,0}$ and velocity $v_{p,0} = -v_{e,0}$, respectively. Hence, energy of emitted particles equals to $W_0 \equiv m_e v_{e,0}^2/2 = m_p v_{p,0}^2/2$, where m_e and m_p are electron and positron masses, respectively. The particles move without collisions in the inter-electrode gap. In addition, we assume that when reaching any electrode, particles are absorbed. The electric potential applied between electrodes U is assumed to be equal to zero.

Let us pass to dimensionless quantities, choosing the particle energy W_0 and Debye–Hückel length $\lambda_D = [(2\tilde{\varepsilon}_0 W_0)/(e^2 n_{e,0})]^{1/2}$ as energy and length units, respectively (here, e is positron charge, and $\tilde{\varepsilon}_0$ is dielectric permittivity of vacuum). Dimensionless coordinate, electric potential, and electric field strength are defined as $\zeta = z/\lambda_D$, $\eta = e\Phi/(2W_0)$ and $\varepsilon = eE\lambda_D/(2W_0)$, respectively.

Stationary solutions are completely determined by three dimensionless parameters: inter-electrode distance $\delta = d/\lambda_D$, potential applied between the electrodes $V = eU/(2W_0)$, and the electric field strength ε_0 at the left electrode. It is convenient to represent these solutions by points of (ε_0, δ) plane for a fixed V value. These points form separate curves, i.e., the solution branches.[10] Such branches are shown in Fig. 1 at $V = 0$.

In the case when $V = 0$ and particles enter the diode from opposite electrodes with the same masses, kinetic energies, and charges (of opposite signs), the total electric charge in the inter-electrode space should be equal to zero, and potential distributions (PD) should be odd-symmetrical with respect to inter-electrode gap center.[11] Taking into account this symmetry allows us to reduce the number of solution branches in comparison with the general case $V \neq 0$.[10] This property will also allow us to correct numerical calculation when studying time-dependent processes within the diode.

Stationary solutions are characterized by wavy form PDs. In Fig. 1, the branches corresponding to the regime without particle reflection from potential barriers are marked as n_k with index k being the number of PD extremes. In the case of particle reflection, we term minimum of PD as virtual electron emitter (e-VE) and maximum of PD as virtual positron emitter (p-VE). If particle reflection occurs, there are two kinds of PD. When e-VE is located to the left of p-VE, the relevant branches are marked as d_k (here, index k is the number of extremes of PD between e-VE and p-VE) in Fig. 1. When, by contrast, e-VE is located to the right of p-VE, the relevant branches are marked as $d_{i,j}$ (here, index i is the number of the PD minima to the left of p-VE, and index j is the number of the PD maxima to the right of e-VE) in Fig. 1. In the case of $V = 0$, only solutions corresponding to branches n_k and d_k with even index k values ($k = 0, 2, 4, \ldots$) and those corresponding branches $d_{s,s}$ with $s = 0, 1, \ldots$ can exist due to symmetry.

In the present paper, we study the stability features of inhomogeneous stationary solutions without particle reflection, i.e., solutions corresponding to n_k branches at $k = 2, 4, \ldots$ (see Fig. 2). Following Ref. 11, we consider the evolution of small PD perturbation. To do this, we write PD in the form

$$\eta(\zeta, \tau) = \eta_0(\zeta) + \tilde{\eta}(\zeta) \exp(-i\Omega\tau), \quad |\tilde{\eta}(\zeta)| \ll |\eta_0(\zeta)|. \quad (1)$$

Here, $\eta_0(\zeta)$ is the unperturbed PD, $\tilde{\eta}(\zeta)$ is the amplitude of PD perturbation, τ is the dimensionless time, and $\Omega = \omega + i\Gamma$ is the complex frequency.

The equation for amplitude of PD perturbation $\tilde{\eta}(\zeta)$ is obtained by linearization of the Poisson's equation in which densities of charged particles moving in time-dependent electric field and the PD (1) are substituted. In the case of regime without reflection of charged particles from potential extremes, this equation is derived in Ref. 11,
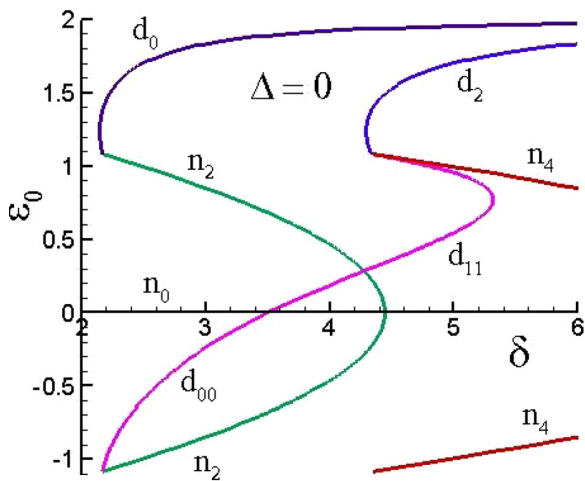
FIG. 1. Branches of stationary solutions in the case of monoenergetic charged particle beams at $V = 0$.
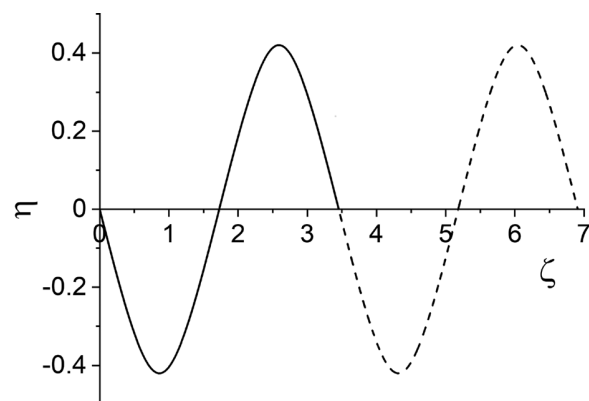
FIG. 2. Typical PD inherent in n_2 branch (solid curve) and n_4 one (solid + dashed curve) at $V = 0$.

$$\tilde{\eta}'(\zeta) + \int_0^\zeta dx \, [u_{e,0}(x)]^{-3} \int_0^x dy \, \tilde{\eta}'(y) \exp\{i\Omega[\sigma_e(\zeta) - \sigma_e(y)]\}$$
$$+ \int_\zeta^\delta dx \, [u_{p,0}(x)]^{-3} \int_x^\delta dy \, \tilde{\eta}'(y) \exp\{i\Omega[\sigma_p(\zeta) - \sigma_p(y)]\}$$
$$= \tilde{\eta}'(\delta) + \int_0^\delta dx \, [u_{e,0}(x)]^{-3} \int_0^x dy \, \tilde{\eta}'(y) \exp\{i\Omega[\sigma_e(\delta) - \sigma_e(y)]\}. \tag{2}$$

Here, $u_{e,0}$, $u_{p,0}$, σ_e, and σ_p are electron and positron velocities at point ζ and times of flight from this point to corresponding electrode in unperturbed potential, respectively. These values are defined as

$$u_{e,0}(\zeta) = [1 + 2\eta_0(\zeta)]^{1/2}, \quad u_{p,0}(\zeta) = [1 - 2\eta_0(\zeta)]^{1/2},$$
$$\sigma_e(\zeta) = \int_0^\zeta dx \, [u_{e,0}(x)]^{-1}, \quad \sigma_p(\zeta) = \int_\zeta^\delta dx \, [u_{p,0}(x)]^{-1}. \tag{3}$$

By solving Eq. (2) with initial condition $\tilde{\eta}(0; \Omega) = 0$, it is possible to find the expression for potential perturbation $\tilde{\eta}(\zeta)$. Boundary condition at the right electrode,

$$\tilde{\eta}(\delta; \Omega) = 0, \tag{4}$$

gives us dispersion equation, whose solutions determine the relation of eigenfrequency Ω with dimensionless inter-electrode length δ (i.e., so-called dispersion branches). In the case when the growth rate $\Gamma = \text{Im}\,\Omega$ is positive, the stationary solution is unstable.

III. SOLUTIONS OF DISPERSION EQUATION

First of all, we solve equation for amplitude of electric field perturbation (2). After changing the order of integration in double integrals and introducing a new function $\varphi(\zeta) = \tilde{\eta}'(\zeta)$, this equation may be rewritten as

$$\varphi(\zeta) + \int_0^\zeta dy \, \exp\{i\Omega[\sigma_e(\zeta) - \sigma_e(y)]\} \, \varphi(y) \int_y^\zeta dx \, [u_{e,0}(x)]^{-3}$$
$$+ \int_\zeta^\delta dy \, \exp\{i\Omega[\sigma_p(\zeta) - \sigma_p(y)]\} \, \varphi(y) \int_\zeta^y dx \, [u_{p,0}(x)]^{-3}$$
$$= \varphi(\delta) + \int_0^\delta dy \, \exp\{i\Omega[\sigma_e(\delta) - \sigma_e(y)]\} \, \varphi(y) \int_y^\delta dx \, [u_{e,0}(x)]^{-3}. \tag{5}$$

Thus, our problem is reduced to solving the Fredholm integral equation of the second kind with respect to function $\varphi(\zeta)$. Since the solution of Eq. (5) is defined up to multiplicative constant $\varphi(\delta)$, we assume that $\varphi(\delta) = 1$. Next, we introduce the notations

$$K(\zeta, y; \Omega) = P(\zeta, y) \, Q(\zeta, y; \Omega),$$

$$P(\zeta, y) = \begin{cases} \int_y^\zeta dx \, [u_{e,0}(x)]^{-3}, & y \le \zeta, \\ \int_\zeta^y dx \, [u_{p,0}(x)]^{-3}, & y \ge \zeta, \end{cases} \tag{6}$$

$$Q(\zeta, y; \Omega) = \begin{cases} \exp\{i\Omega[\sigma_e(\zeta) - \sigma_e(y)]\}, & y \le \zeta, \\ \exp\{i\Omega[\sigma_p(\zeta) - \sigma_p(y)]\}, & y \ge \zeta. \end{cases}$$

Then Eq. (5) may be rewritten as

$$\varphi(\zeta; \Omega) + \int_0^\delta dy \, K(\zeta, y; \Omega) \, \varphi(y; \Omega) - \int_0^\delta dy \, K(\delta, y; \Omega) \, \varphi(y; \Omega) = 1. \tag{7}$$

If the solution of Eq. (7) is found, then it is enough to integrate the function $\varphi(\zeta; \Omega)$ to obtain the amplitude of potential perturbation,

$$\tilde{\eta}(\zeta; \Omega) = \int_0^\zeta dy \, \varphi(y; \Omega) + \tilde{\eta}(0; \Omega).$$

At the right boundary, we have

$$\tilde{\eta}(\delta; \Omega) = \int_0^\delta dy \, \varphi(y; \Omega) + \tilde{\eta}(0; \Omega). \tag{8}$$

Since the potential values on the electrodes are fixed, the equalities $\tilde{\eta}(0; \Omega) = 0$, $\tilde{\eta}(\delta; \Omega) = 0$ take place, and Eq. (8) gives us the dispersion equation

$$\int_0^\delta dy \, \varphi(y; \Omega) = 0. \tag{9}$$

Analysis of solution of Eq. (9) allows us to determine the stability features of stationary solutions with inhomogeneous PD. Hence, in order to get dispersion equation, it is necessary to find the function $\varphi(\zeta; \Omega)$ by solving Eq. (7).

Since it is impossible to find an analytical solution to this equation, we use an approximate numerical method. To this end, we divide the interval $[0, \delta]$ into subintervals of length h by points ζ_i, $i = 0, 1, \ldots N$, where $0 = \zeta_0 < \zeta_1 < \cdots < \zeta_N = \delta$ and replace the integrals in Eq. (6) with sums by the trapezoid method. This procedure leads to a system of linear equations with respect to the quantities, $\varphi_i(\Omega) = \varphi(\zeta_i; \Omega)$, $i = 0, 1, \ldots, N - 1$,

$$\varphi_i + h \sum_{j=1}^{N-1} [K(\zeta_i, \zeta_j; \Omega) - K(\delta, \zeta_j; \Omega)] \, \varphi_j$$
$$+ \frac{h}{2} \{[K(\zeta_i, 0; \Omega) - K(\delta, 0; \Omega)] \, \varphi_0$$
$$+ K(\zeta_i, \delta; \Omega) - K(\delta, \delta; \Omega)\} = 1. \tag{10}$$

Here, we take into account that $\varphi_N = 1$.

Assume that the solution of Eq. (10) is found. Then, substituting it into the dispersion Eq. (9) gives

$$h \sum_{j=1}^{N-1} \varphi_j(\delta, \Omega) + \frac{h}{2} [\varphi_0(\delta, \Omega) + 1] = 0. \tag{11}$$

This equation allows us to obtain eigenfrequencies as well as both aperiodic and oscillation dispersion branches.

Aperiodic dispersion branches, corresponding to n_2 and n_4 branches, are shown in Fig. 3. The n_0 branch calculated by the method described above is also shown in Fig. 3. It fully coincides with the branch n_0 obtained in Ref. 11 on the base of analytical solution of Eq. (7). Figure 3 shows that the stationary solutions corresponding to n_2 branch are aperiodically unstable (the growth rate $\Gamma > 0$). It is also shown that all oscillating modes corresponding to n_2 branch have negative growth rate.

As for solutions belonging to n_4 branch, we see that relevant stationary states are aperiodically stable within interval $6.766 < \delta < 7.752$.
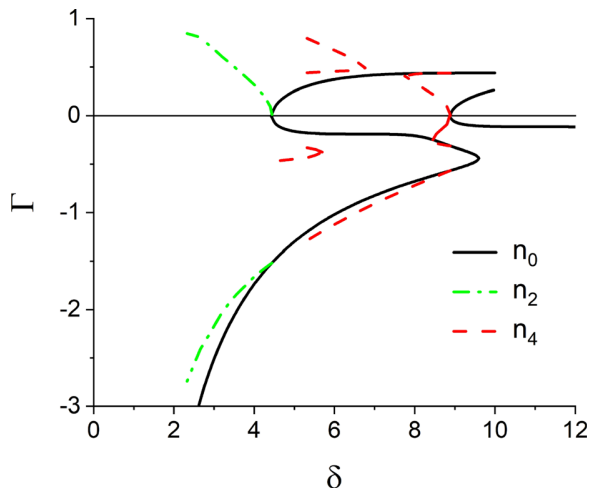
FIG. 3. Aperiodic dispersion branches, corresponding to n_0, n_2, and n_4 branches.

However, the consideration of oscillating branches in this interval shows that one of them has positive growth rate; hence, these stationary states are also unstable with respect to small oscillating perturbations (see Fig. 4). Thus, all the solutions corresponding to n_2 and n_4 branches are unstable.

Calculations of dispersion curves show that dependencies $\Gamma(\delta)$ for the PDs belonging to the same n_k branch with different signs of field at the left boundary, ε_0, coincide in the case of $V = 0$. It is true for both aperiodic and oscillating branches. This can be proved in the general case.

Thus, our investigations show that inhomogeneous stationary solutions corresponding to n_2 and n_4 branches are unstable, i.e., such stationary solutions cannot exist. It is possible to suppose that stationary solutions, corresponding to n_{2s} branches with $s \geq 3$, are also unstable with respect to small perturbations. It should be pointed out that the instability has the same mechanism as well-known Pierce instability, when electron beam moves through background of immobile ions in the diode space.[11] In Sec. IV, we show what solutions may appear instead of the unstable stationary solutions.
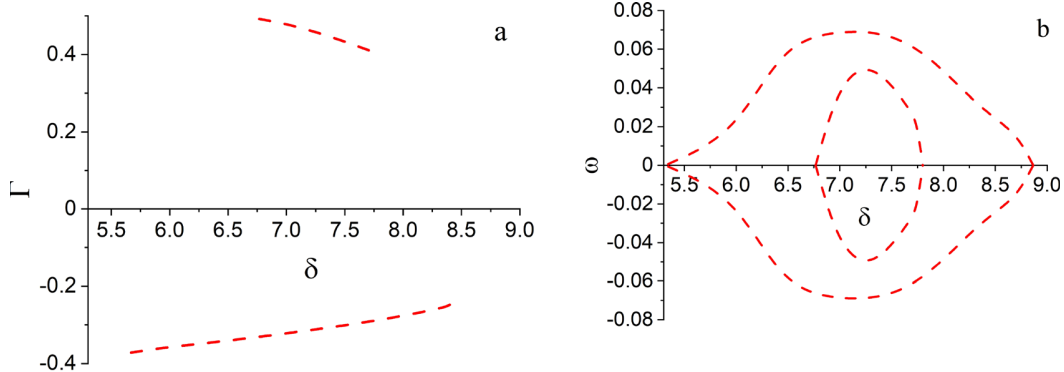
Note that while finding the eigenfrequencies for given δ by solving (11), we also get a set of eigenmodes [i.e., solutions of the system (10)] relevant to these frequencies. Thus, expanding an arbitrary potential perturbation in terms of eigenmodes, we can predict the potential distribution evolution at the initial stage where our consideration is relevant. Evidently, if there is the eigenfrequency whose positive real part is significantly larger than those of other eigenfrequencies, then, after a short time, the corresponding mode will be the main term that determines the shape of the potential distribution deviation from the stationary one. This shape remains unchanged over time, and the deviation of potential distribution in the diode from the steady-state one will exponentially grow, exponent being the real part of eigenfrequency. This is exactly what we have obtained as a result of independent numerical simulation of small perturbation evolution described in Sec. IV.

IV. NUMERICAL STUDY OF INSTABILITY DEVELOPMENT

When studying steady-state solution stability features in the diode numerically, we calculate the evolution of small perturbation of an electric field stationary distribution. The eigenmode growth rate Γ and frequency ω are evaluated from time dependence of any characteristic of this process (e.g., electric field strength at the left electrode). If the solution turns out to be unstable, the perturbation evolution leads to solution deviation from the stationary one ($\Gamma > 0$). In the opposite case ($\Gamma < 0$), the solution returns to the stationary one.

In contrast to Sec. III, where solution stability features were studied analytically, the electron and positron flows should not be monoenergetic in numerical modeling. We choose their velocity distribution functions (VDFs) on electrodes in the form of "gates" of small width $\Delta \ll 1$,

$$f_0^{(e)}(u) = \begin{cases} (2\Delta)^{-1}, & u \in [1 - \Delta, 1 + \Delta], \\ 0, & u \in (0, 1 - \Delta) \cup (1 + \Delta, \infty), \end{cases} \quad (12)$$

$$f_0^{(p)}(u) = \begin{cases} (2\Delta)^{-1}, & u \in [-1 - \Delta, -1 + \Delta], \\ 0, & u \in (-\infty, -1 - \Delta) \cup (-1 + \Delta, 0). \end{cases} \quad (13)$$

When using the charged particle VDFs in the form (12) and (13), stationary solutions should slightly differ from those used in the linear theory with δ-shaped VDFs. We have computed new stationary distributions of the electric field.

FIG. 4. Oscillating dispersion branches for solutions corresponding to n_4 branch. Growth rates Γ and eigenfrequencies ω are shown on panels (a) and (b), respectively.

In this paper, we study the mode without reflection of particles from potential barriers, namely, the stability features of solutions belonging to the branches n_{2i}. For these solutions, the particle density are determined by the following formulas:

$$n_{e,p}(\eta) = \frac{1}{2\Delta}\left[\sqrt{(1+\Delta)^2 \pm 2\eta} - \sqrt{(1-\Delta)^2 \pm 2\eta}\right]. \quad (14)$$

Here, signs "+" and "−" relate to electrons and positrons, respectively.

Substituting the particle densities (14) into the Poisson's equation, multiplying both sides by η' and integrating the result over the potential from η_1 to η, we obtain

$$\eta' = \pm\left\{(\eta'_1)^2 + \frac{1}{3\Delta}[D_0(\eta) - D_0(\eta_1)]\right\}^{1/2}. \quad (15)$$

Here,

$$D_0(\eta) = \left[(1+\Delta)^2 + 2\eta\right]^{3/2} - \left[(1-\Delta)^2 + 2\eta\right]^{3/2}$$
$$+ \left[(1+\Delta)^2 - 2\eta\right]^{3/2} - \left[(1-\Delta)^2 - 2\eta\right]^{3/2}. \quad (16)$$

Next, we integrate Eq. (15) and calculate the potential and electric field distributions. We use the electric field strength at the left boundary as a parameter.

Relationship between ε_0 and the potential minimum η_m is derived from Eq. (15) if we substitute $\eta = 0$ and $\eta_1 = \eta_m$ in it,

$$\varepsilon_0 = \left(4 + \frac{4}{3}\Delta^2 - \frac{1}{3\Delta}\left\{\left[(1+\Delta)^2 + 2\eta_m\right]^{3/2}\right.\right.$$
$$- \left[(1-\Delta)^2 + 2\eta_m\right]^{3/2} + \left[(1+\Delta)^2 - 2\eta_m\right]^{3/2}$$
$$\left.\left.- \left[(1-\Delta)^2 - 2\eta_m\right]^{3/2}\right\}\right)^{1/2}. \quad (17)$$

The limiting value of ε_0 for the n_2 branch is reached at $\eta_m = -(1-\Delta)^2/2$ (for lesser η_m, particle reflection begins),

$$\varepsilon_0 = \left(4 - \frac{4}{3}\left[\sqrt{2} + 2\sqrt{\Delta} - \sqrt{2}\Delta - \Delta^2 + \frac{\sqrt{2}(1+\Delta^2)}{1-\Delta+\sqrt{1+\Delta^2}}\right]\right)^{1/2}.$$

For $\Delta \to 0$, this formula yields an equation corresponding to the case of monoenergetic beams: $\varepsilon_0 = [2(2-\sqrt{2})]^{1/2} \approx 1.0824$, here $\eta_m = -1/2$.

The minimum point position ζ_m is found by integrating Eq. (15) from η_m to zero,

$$\zeta_m = \sqrt{3\Delta}\int_{\eta_m}^0 \frac{dx}{[D_0(x) - D_0(\eta_m)]^{1/2}}. \quad (18)$$

It can be seen from Eq. (14) that the PD is symmetric with respect to the point $\zeta = \zeta_m$. Hence, the gap middle is at $\zeta = 2\zeta_m$ point and the gap value for n_2 branch is

$$\delta = 4\zeta_m(\varepsilon_0). \quad (19)$$

Here, ζ_m is defined by Eq. (18), with η_m being expressed in terms of ε_0 from Eq. (17).

The upper part of the n_2 branch is constructed according to Eqs. (17)–(19) by varying η_m from 0 to $-(1-\Delta)^2/2$, and the lower part is

obtained by merely mirror reflection of the upper part about the $\varepsilon_0 = 0$ axis.

The PD in the diode for the solutions corresponding to the n_2 branch on the segment $(0, \zeta_m)$ for a given value of δ is found by integrating Eq. (15) with the boundary condition $\eta(0) = 0$. In this case, the minimum coordinate ζ_m, the minimum potential η_m, and ε_0 are determined from the relations (17)–(19). On the segment $(\zeta_m, \delta/2)$, the PD is constructed by mirror reflection about the $\zeta = \zeta_m$ line, and on the segment $(\delta/2, \delta)$, it is found from the condition of solution antisymmetry with respect to the $\delta/2$ point. Branches with large index values are easy to get from these solutions by adding the integer number of waves.

For modeling the evolution of electric field and charged particle VDFs, we used two different numerical codes: PIC-code and EK-code. When modeling VDFs in PIC-code, individual particles moving in an electric field specified at the grid nodes are considered. In total, the grid contains N_ζ equally spaced nodes with distance $h_\zeta = \delta/(N_\zeta - 1)$ between them. The cloud-in-cell model is used to find charge density at the grid nodes (linear contribution of a particle to density in neighboring nodes),[19] and density of a unit value corresponds to N_0 particles in a cell. To calculate the electric field at the grid nodes, the Poisson's equation is solved, and linear approximation is used for the field between nodes.[19] To find the position of the particles at the next time moment, the "leapfrog method" is used.[19] Time step h_τ is chosen to be constant. At the end of every step, the particles that hit the electrodes are discarded, and particles coming from the electrodes are added. In this case, the added electrons and positrons are taken with arbitrary velocities uniformly distributed in the $[1-\Delta, 1+\Delta]$ and $[-1-\Delta, -1+\Delta]$ intervals [Eqs. (12) and (13)], and time moments of their leaving the electrode are distributed uniformly over the h_τ interval.

As the initial field distribution at time moment $\tau = \tau_0$, a stationary distribution evaluated according to the algorithm described above is set with a perturbation $\tilde\eta(\zeta, \tau_0) = C\sin(2\pi\zeta/\delta)$ ($C \ll 1$) imposed on it. Sometimes, we set $C = 0$; in this case, perturbation is due to numerical error. Initial particle VDFs in perturbed stationary field $f^{(a)}|_{t=0}$, $a = e, p$ are defined by the relations

$$f^{(a)}(\zeta, u)|_{t=0} = \frac{1}{2\Delta} \quad \text{if } u \in \left[u_{\min}^{(a)}(\zeta), u_{\max}^{(a)}(\zeta)\right],$$
$$f^{(a)}(\zeta, u)|_{t=0} = 0 \quad \text{if } u \in \left(-\infty, u_{\min}^{(a)}(\zeta)\right] \cup \left[u_{\max}^{(a)}(\zeta), +\infty\right). \quad (20)$$

Here, $a = e, p$, and

$$u_{\min}^{(a)}(\zeta) = -s\sqrt{(-s-\Delta)^2 + 2s(\eta_0(\zeta) + \tilde\eta(\zeta, \tau_0))}, \quad (21)$$

$$u_{\max}^{(a)}(\zeta) = -s\sqrt{(-s+\Delta)^2 + 2s(\eta_0(\zeta) + \tilde\eta(\zeta, \tau_0))} \quad (22)$$

and $s = -1$ for electrons, and $s = 1$ for positrons. It is seen from Eq (20) that the VDFs for electrons and positrons at $t = 0$ have a form of "gates" for each point ζ of inter-electrode gape, ie., VDFs are constant over a certain range of velocities and vanish outside of it. To start the calculation in PIC code some amount of N_i^a of particle (electrons and positrons) is added in each cell. Denote the boundaries of the cell i by $\zeta_i = h_\zeta(i-1)$, $\zeta_{i+1} = h_\zeta i$. The amount $N_i^{(a)}$ is

$$N_i^{(a)} = h_\zeta(u_{\max}^{(a)}(\zeta_{i+1/2}) - u_{\min}^{(a)}(\zeta_{i+1/2}))/(2\Delta). \quad (23)$$

Here i is the number of the cell, $\zeta_{i+1/2} = \zeta_i + h_\zeta/2$. The coordintes and velocities of the particles are uniformly distributed over interval

$[\zeta_i, \zeta_{i+1}]$ and over the velocity range $[u_{\min}^{(a)}(\zeta_{i+1/2}), u_{\max}^{(a)}(\zeta_{i+1/2})]$. Furthermore, the charge densities are evaluated, and the Poisson's equation is solved, and new positions of particles are calculated, whereupon the process is repeated.

The algorithm of EK-code modified for the case when negative and positive charged particles enter from different electrodes with VDFs (12) and (13) is described thoroughly in Refs. 17 and 18. It is based on sequential calculation of the charged particle VDFs, densities, and electric field distribution at each time step. When evaluating the particle VDFs in each node of the spatiotemporal grid, a certain set of particle trajectories is computed. In the course of calculation, a trajectory of each particle is traced back in time in an electric field, whose distribution is known at all previous time moments up to the moment when the particle left the electrode. The field distribution at each time moment is the Poisson's equation solution, whose right side contains the electron and positron densities calculated from the VDFs at the moment. To ensure self-consistency of calculations, we perform iterations at each time step.

When computing small perturbation development using the EK-code, the electric field distribution is considered to be equal to the stationary one during the time interval $(0, \tau_0)$. In the simulations described as follows, we chose $\tau_0 = 18$. Since the time moment following the $\tau = \tau_0$ one, we started to evaluate the electric field distribution along with particle distribution in accordance with the algorithm described earlier.

The calculations were carried out for the inter-electrode gap values $\delta = 3$ and $\delta = 4$ for stationary solutions with both positive and negative ε_0 values. Due to numerical errors in the given initial distribution of the stationary field, the iteration process at the first step of self-consistent computation led to a small surge in field distribution at the moment $\tau = \tau_0$, and we considered the following calculations as a modeling of the perturbed stationary solution evolution. Figure 5 shows the time dependences for the maximum difference $\tilde{\eta}(\zeta, \tau) = \eta(\zeta, \tau) - \eta_0(\zeta)$ for $\varepsilon_0(\tau_0) > 0$ and $\varepsilon_0(\tau_0) < 0$ for $\delta = 4$ at the initial stage of evolution, where linear theory is applicable. After a brief transient process, the maximum $\tilde{\eta}_M(\tau)$ value increases exponentially with growth rate $\Gamma = 0.32$ in both cases. This agrees well with the growth rate provided by a semi-analytical method for monoenergetic beams

($\Gamma = 0.31$). Similar calculations for $\delta = 3$ give $\Gamma = 0.68$, which coincides with the value obtained using the semi-analytical method.

Moreover, we compared a form of computed perturbation with that predicted by linear theory. In the region of exponential growth, one can select an area where the perturbation form mostly does not change and coincides with that of the fastest aperiodic growing mode (the main eigenmode). Figure 6 shows $\tilde{\eta}(\zeta, \tau)$ dependences computed via EK-code for positive and via PIC-code for negative $\varepsilon_0(\tau_0)$ values normalized to the maximum of the main eigenmode, in the time interval where the linear theory is relevant. When evaluated by EK-code, this is the range of values $\tau - \tau_0$, approximately 3–7 for $\delta = 3$ and 4–20 for $\delta = 4$, and when calculated by PIC-code, it is 5–7 for $\delta = 3$ and 11–19 for $\delta = 4$. One can see that the perturbation form obtained numerically changes little and fits with that calculated analytically. The area of applicability of the linear theory begins with the termination of the transient process (minor modes decay) and ends with the perturbation amplitude increase for values of the order of several hundredths.

Our simulations revealed four possible evolution scenarios, which were of the same nature for $\delta = 3$ and $\delta = 4$. The first and the second
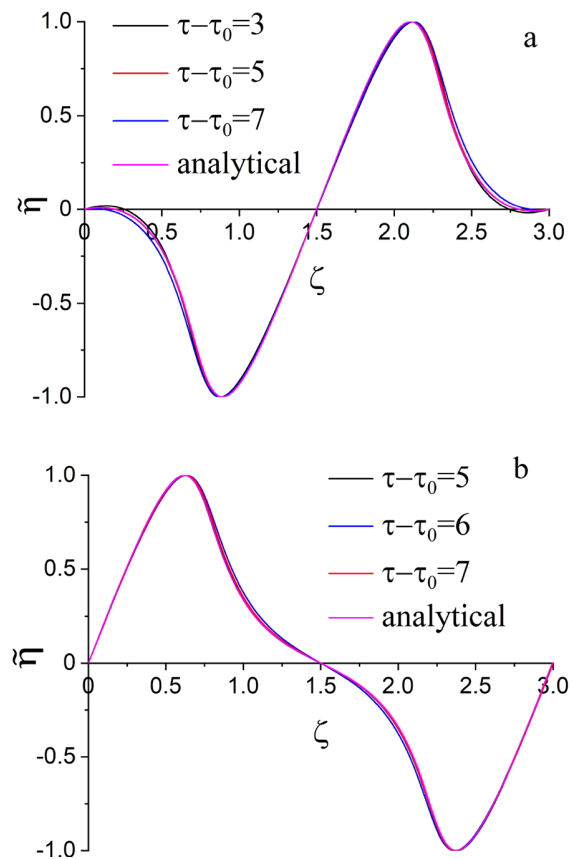
FIG. 6. Comparison of dependences $\tilde{\eta}(\zeta, \tau)$ obtained as a result of numerical simulations with main eigenmodes found by semi-analytical method for a set of time moments: (a) $\varepsilon_0(\tau_0) < 0$, calculation via EK-code and (b) $\varepsilon_0(\tau_0) > 0$, calculation via PIC-code; $\delta = 3$.

FIG. 5. Dependences $\tilde{\eta}_M(\tau)$ for $\varepsilon_0 > 0$ (solid lines) and $\varepsilon_0 < 0$ (dashed lines), computed by EK-code (1) and PIC-code (2); $\delta = 4$.

ones correspond to the potential maximum $\eta_M(\tau)$ growth during linear stage of the evolution process with $\varepsilon_0(\tau_0) > 0$ and $\varepsilon_0(\tau_0) < 0$, respectively. The third and the fourth ones correspond to $\eta_M(\tau)$ decreasing during linear stage with $\varepsilon_0(\tau_0) > 0$ and $\varepsilon_0(\tau_0) < 0$, respectively.

In the first and second cases after leaving the area of linear theory applicability, the distribution maximum proceeds to increase and eventually reaches the values at which charged particle reflection begins. In the first case after entering the mode with reflection, $\varepsilon_0(\tau)$ and $\eta_M(\tau)$ fluctuate around the values corresponding to the d_0 branch. Gradually, the oscillations take on a regular nature, and eventually become periodic. In the second case after passing a certain maximum value $\eta_M(\tau)$ begins to decrease and approaches zero, while the PD takes the form of a curve with two minima and two maxima. The value $\eta_M(\tau) = 0$ is not reached, since the maxima (one of which is placed on the left of the middle of diode, and another, on the right) at some moment become equal and change places. Afterward $\eta_M(\tau)$ performs fluctuations, during which ε_0 changes sign, and PD takes a form of a curve with four extrema near zero. Despite the complex nature of these processes, it can be argued that they are practically independent of initial perturbation. This is confirmed by the fact that the same process repeats in the third case, when $\varepsilon_0(\tau_0) > 0$ and the potential maximum value does not increase, yet decreases during the linear stage of the process. In this case, after leaving the area of linear theory applicability, $\eta_M(\tau)$ proceeds to decrease. As well $\varepsilon_0(\tau)$ decreases, and, at some time moment, it vanishes and afterward changes sign. The PD in the vicinity of zero values of $\varepsilon_0(\tau)$ has four extrema. Then, $\eta_M(\tau)$ increases (PD maximum being in the right part of the diode) and enters the mode with particle reflection. In the course of further PD evolution, the dependence $\eta_M(\tau)$ within the calculation margin of error reproduces the obtained one in the second case. For $\delta = 3$, we followed an evolution of the PD prior to reaching homogeneous solution in the second and the third cases.

Finally, in the fourth case, exponentially damped oscillations of the PD occur in the diode (PD also takes the form of a curve with four extrema of very small values). The solution approaches the homogeneous one with the growth rate predicted by linear theory.[11]

Dependences $\eta_M(\tau)$, obtained using both EK-code and PIC-code, match completely for all described cases. Figure 7 shows dependences $\eta_M(\tau)$ for $\delta = 3$ for all four cases.

V. CONCLUSION

Stability features of the steady-state solutions for a diode with counterstreaming electron and positron flows in the mode without charged particle reflection from potential extrema have been studied. Such solutions belong to the n_{2s} branches with $s = 0, 1, 2, \ldots$ in ε_0, δ-plane (Fig. 1). Homogeneous solutions (n_0 branch) are stable when the inter-electrode gap is less than $\sqrt{2}\,\pi\,\lambda_D$.[11] On the other hand, all solutions lying on the n_2 and n_4 branches are unstable with respect to small perturbations. Thus, we have completed the study of all steady-state solutions without charged particles reflection from potential extrema.

In the course of the research, an equation for electric field perturbation amplitude has been derived. A method for determining stability features of the solutions corresponding to n_k branches with arbitrary value of k has been proposed. Dispersion equations have been obtained, and their solutions were studied. In addition, we have studied stability features of the same steady-state solutions using two
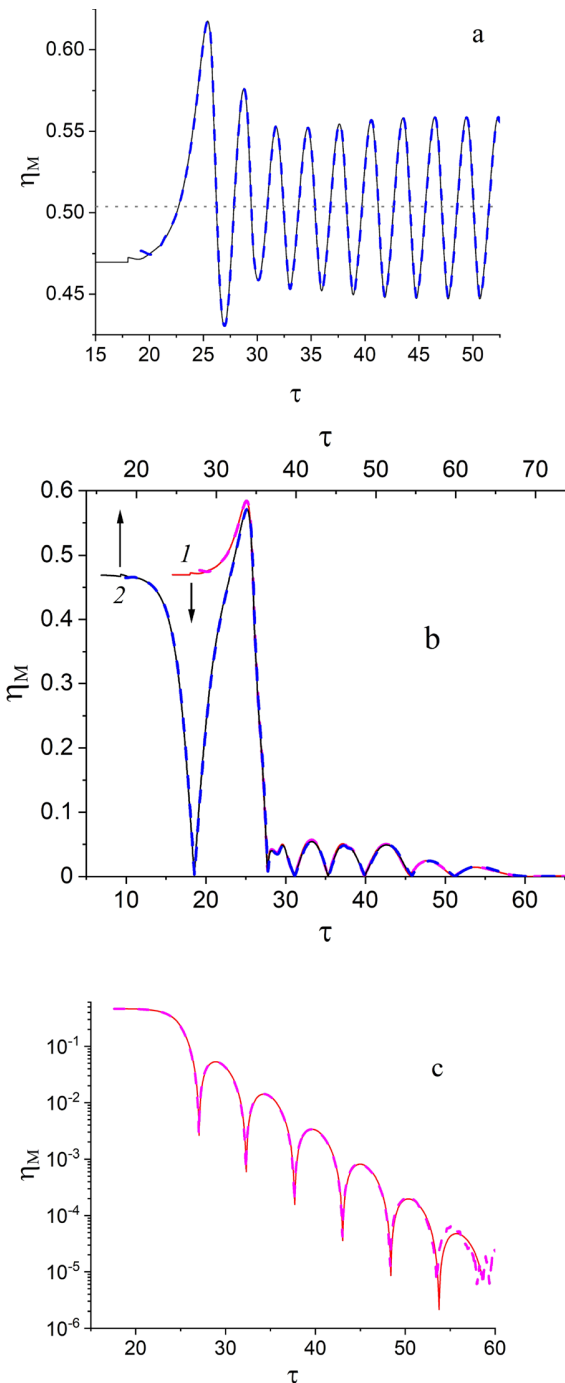
FIG. 7. Dependences $\eta_M(\tau)$ computed via EK-code (solid lines) and via PIC-code (dashed lines) for $\delta = 3$. The graphs differ from each other by $\varepsilon_0(\tau_0)$ sign and the η_M behavior at the early stage of evolution: (a) for $\varepsilon_0(\tau_0) > 0$, η_M increases; (b) for $\varepsilon_0(\tau_0) < 0$, η_M increases (1, bottom axis), and for $\varepsilon_0(\tau_0) > 0$, η_M decreases (2, top axis); and (c) for $\varepsilon_0(\tau_0) > 0$, η_M decreases. The PIC-code curves are shifted along the τ-axis to coincide with EK-code ones. In figure (a), the dotted line shows the η_M magnitude that corresponds to the d_0 branch.

numerical methods: E,K-code and PIC-code. In this case, a small perturbation is added to the steady-state electric field distribution, and its evolution is traced. From the time characteristics of this process, we have found eigenmodes. The results obtained by both codes coincided with one another and also with those obtained analytically.

To complete studying stability features of the steady-state solutions, it is necessary to study those for more complex regime where the charged particles are reflected from the potential barriers (d branches in Fig. 1). An equation for electric field distribution perturbation has not been obtained for this mode hitherto. Therefore, today, the only possibility is to explore the stability features of the solutions, that is, calculation of a small field perturbation evolution using numerical codes. In our next paper, we plan to study the stability features of the steady-state solutions by simulations using the above-mentioned codes.

AUTHOR DECLARATIONS
Conflict of Interest

The authors have no conflicts to disclose.

Author Contributions

Leonid A. Bakaleinikov: Conceptualization (equal); Data curation (equal); Formal analysis (equal); Investigation (equal); Methodology (equal); Supervision (equal); Visualization (equal); Writing – original draft (equal); Writing – review & editing (equal). **Victor I. Kuznetsov:** Conceptualization (equal); Data curation (equal); Formal analysis (equal); Investigation (equal); Methodology (equal); Project administration (equal); Supervision (equal); Validation (equal); Writing – original draft (equal); Writing – review & editing (equal). **Ekaterina Flegontova:** Conceptualization (equal); Data curation (equal); Formal analysis (equal); Investigation (equal); Methodology (equal); Software (equal); Validation (equal); Visualization (equal); Writing – original draft (equal); Writing – review & editing (equal). **Dmitry P. Barsukov:** Data curation (equal); Investigation (equal); Methodology (equal); Software (equal); Visualization (equal); Writing – original draft (equal). **Ivan K. Morozov:** Investigation (equal); Software (equal); Validation (equal); Visualization (equal); Writing – original draft (equal).

DATA AVAILABILITY

The data that support the findings of this study are available from the corresponding author upon reasonable request.

REFERENCES

[1] H. Chen and F. Fiuza, Phys. Plasmas **30**, 020601 (2023).
[2] V. S. Beskin, Phys. Usp. **61**, 353 (2018).
[3] M. Gedalin, D. B. Melrose, and E. Gruman, Phys. Rev. E **57**(3), 3399 (1998).
[4] D. B. Melrose, Plasma Phys. Controlled Fusion **45**(5), 523 (2003).
[5] Y. Lyubarsky, "Pulsar emission mechanisms," AIP Conf. Proc. **983**, 29 (2008).
[6] A. Philippov, A. Timokhin, and A. Spitkovsky, Phys. Rev. Lett. **124**(24), 245101 (2020).
[7] E. A. Tolman, A. A. Philippov, and A. N. Timokhin, Astrophys. J. Lett. **933**(2), L37 (2022).
[8] V. M. Kontorovich and A. B. Flanchik, J. Exp. Theor. Phys. **106**, 869 (2008).
[9] V. M. Kontorovich and A. B. Flanchik, Astrophys. Space Sci. **345**(1), 169 (2013).
[10] A. Ya. Ender, V. I. Kuznetsov, and A. A. Gruzdev, Plasma Phys. Rep. **42**(10), 936 (2016).
[11] V. I. Kuznetsov, L. A. Bakaleinikov, and E. Yu. Flegontova, Phys. Plasmas **29**(22), 112115 (2022).
[12] A. Ya. Ender, V. I. Kuznetsov, H. Schamel, and P. V. Akimov, Phys. Plasmas **11**(6), 3212 (2004).
[13] K. Qu, S. Meuren, and N. J. Fisch, Phys. Plasmas **29**, 042117 (2022).
[14] K. Arshad, F. Siddique, A. M. Mirza, and Aman-ur-Rehman, Astrophys. Space Sci. **350**(1), 169 (2014).
[15] K. Arshad, F. Siddique, A. M. Mirza, and Aman-ur Rehman, Astrophys. Space Sci. **350**(2), 585 (2014).
[16] K. Arshad and S. Poedts, Phys. Plasmas **27**(12), 122904 (2020).
[17] V. I. Kuznetsov and A. Ya. Ender, Plasma Phys. Rep. **36**(3), 226 (2010).
[18] V. I. Kuznetsov, E. Yu. Flegontova, and L. A. Bakaleinikov, Phys. Plasmas **27**, 092304 (2020).
[19] R. W. Hockney and J. W. Eastwood, *Computer Simulation Using Particles* (Taylor and Francis Group, New York/London, 1988).

22 January 2024 12:51:34